UCRL-JC-130948
PREPRINT

Progress in Understanding the Short-pulse-driven Collisional X-ray Lasers

J. Nilsen, Y. Li, J. Dunn, A. L. Osterheld

This paper was prepared for submittal to the
6th International Conference on X-ray Lasers
Kyoto, Japan
August 31-September 4, 1998

September 21, 1998

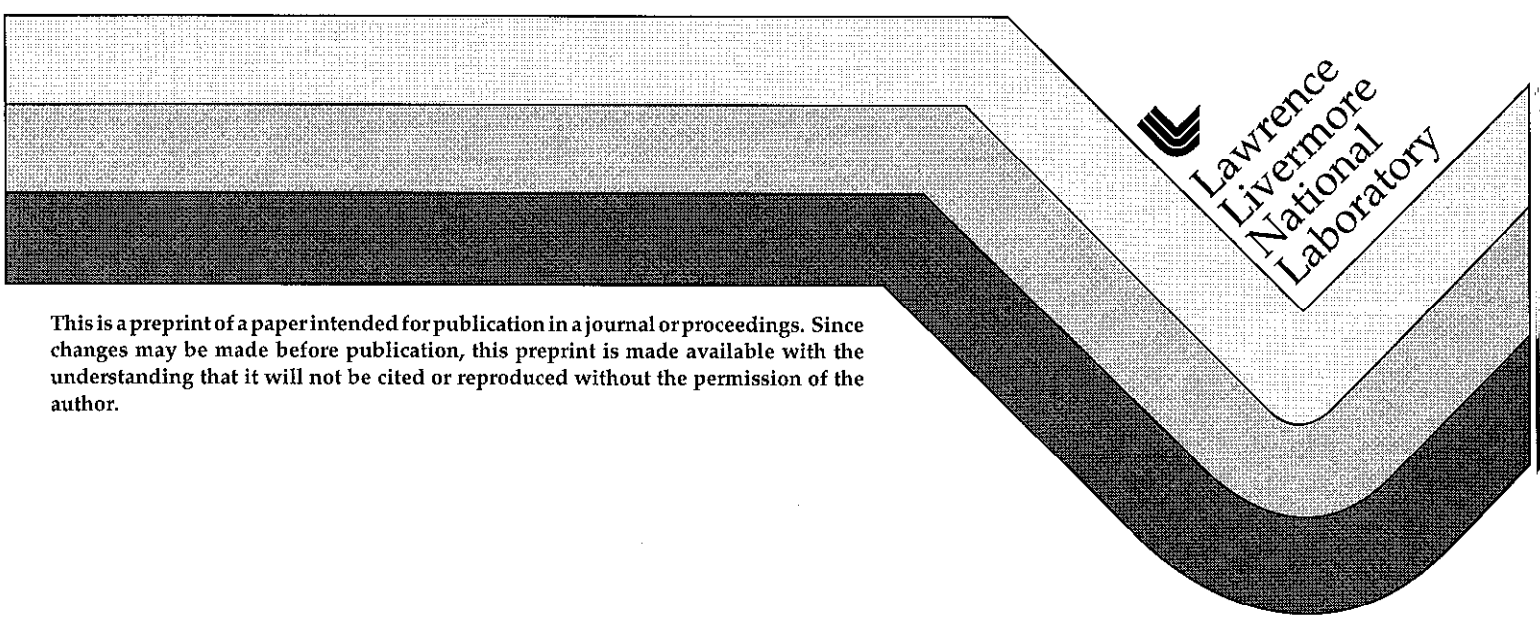

Progress in understanding the short-pulse-driven collisional X-ray lasers

Joseph Nilsen, Yuelin Li, James Dunn, and Albert L. Osterheld

Lawrence Livermore National Laboratory, Livermore, CA 94550

Abstract. Recently, the technique of using a nsec pulse to preform and ionize the plasma followed by a psec pulse to heat the plasma has enabled low-Z neon-like and nickel-like ions to lase driven by small lasers with only ten joules of energy. In this work we model recent experiments done using the COMET laser at LLNL to illuminate 1 cm long slab targets of Ti with a 4.8 J, 800 ps prepulse followed 1.6 nsec later by a 6 J, 1 psec drive pulse. The LASNEX code is used to calculate the hydrodynamic evolution of the plasma and provide the temperatures and densities to the XRASER code, which then does the kinetics calculations to determine the gain. The temporal and spatial evolution of the plasma is studied both with and without radiation transport included for the 3d and 3s $\rightarrow$ 2p Ne-like Ti resonance lines. Large regions with gains greater than 80 cm^{-1} are predicted for the $3p\ ^1S_0 \rightarrow 3s\ ^1P_1$ Ne-like Ti laser line at 326 Å. Given the large gain and large gradients in these plasmas, we do propagation calculations including refraction to understand which regions have the right combination of high gain and low gradients to contribute to the X-ray laser output. Calculations are also presented using different delays between the long and short pulse and different widths for the short pulse to provide better insight for optimizing the laser output. In addition to the standard 326 Å laser line, high gain is also predicted and observed for the $3d\ ^1P_1 \rightarrow 3p\ ^1P_1$ laser line at 301 Å in Ne-like Ti. We present calculations with and without radiation transport included on the strong $3d\ ^1P_1 \rightarrow 2p\ ^1S_0$ resonance line to better understand this self photopumping effect. We also look at the analog transition in Ni-like ions to understand if self photopumping may also play a role in Ni-like ions. High gain is predicted on the $3d^9\ 4f\ ^1P_1 \rightarrow 3d^9\ 4d\ ^1P_1$ Ni-like transition and this line has recently been observed at 226 Å in Ni-like Mo.

1. Introduction

Since the introduction of the prepulse or multiple pulse technique [1,2] most researchers now use some variant of these techniques. As a result the Ne-like $3p\ ^1S_0 \rightarrow 3s\ ^1P_1$ laser line now dominates the laser output as was originally predicted over 20 years ago. These techniques illuminate solid targets with several pulses, with the first pulse used to create a larger, more uniform preplasma which is at the right densities for gain and laser propagation and which allows the subsequent pulses to be absorbed more efficiently. Typical pulse durations are 100 ps for the multiple pulse technique and up to 1 ns for the prepulse technique and typically use 100 to 1000 J of energy. In the above techniques the pulse duration is held constant but the contrast and separation between pulses is varied. A recent variant of these techniques, which uses less than 10 J of energy, is the use of a nsec prepulse followed by a psec drive pulse to demonstrate lasing at 326 Å in Ne-like Ti at the Max Born Institute (MBI) [3]. The Ti experiments were reproduced at Lawrence Livermore National

Laboratory (LLNL) using the COMET laser and extended to Ni-like Pd at 146 Å [4]. In this paper we model the Ne-like Ti experiments done with the COMET laser to understand the plasma conditions present and what gain is possible on different transitions. In addition to the Ne-like Ti 3p $^1S_0 \rightarrow$ 3s $^1P_1$ transition at 326 Å we discuss the photopumping mechanism [5,6] which drives the gain of the Ne-like Ti 3d $^1P_1 \rightarrow$ 3p $^1P_1$ transition at 301 Å.

2. Plasma Modeling

To estimate what gain might be achieved on various transitions in Ne-like Ti we did LASNEX one dimensional (1D) computer simulations to model a Ti slab illuminated by a 4.8 J, 800 psec gaussian pulse followed 1.6 nsec later by a 6 J, 1 psec gaussian pulse from a 1.05 μm Nd laser. The laser is focused to a 50 μm wide by 1.2-cm long line. The 1.6 nsec delay between the long and short pulse is peak to peak. This is similar to the conditions used to demonstrate lasing in Ne-like Ti and Ni-like Pd at the COMET laser facility. The LASNEX calculations include an expansion angle of 15 degrees in the dimension perpendicular to the primary expansion so as to simulate 2D effects.

Using the LASNEX calculated densities and temperatures as input to the XRASER code, the gains of the laser lines were calculated including radiation trapping effects for the four strong 3d and 3p $\rightarrow$ 2p resonance lines in Ne-like Ti. Bulk Doppler effects due to the expansion of the plasmas were also included. The XRASER atomic model includes all 89 detailed levels for levels up to n = 4 in Ne-like Ti.

Calculations predict four dominant laser lines. These can be divided into two classes. First there is the 3p $^1S_0 \rightarrow$ 3s $^1P_1$ line at 326 Å and the 3p $^1S_0 \rightarrow$ 3s $^3P_1$ line at 285 Å. These lines share the same upper laser level which is populated by monopole collisional excitation

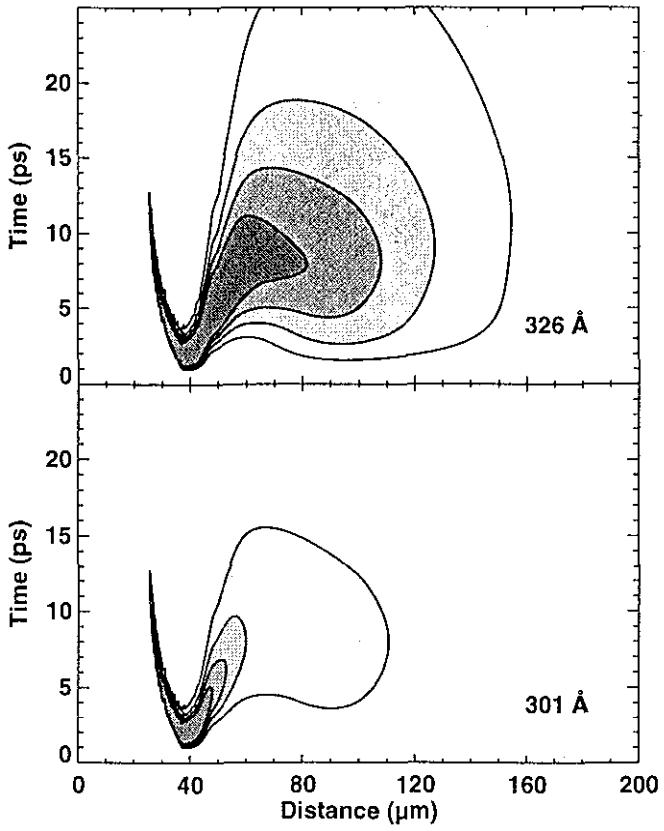

Fig. 1. Spatial and temporal evolution of the gain for Ne-like Ti laser lines. Contours represent gain > 80, 60, 40, and 20 cm^{-1}. The short pulse laser drive peaks at 1 ps on this time scale.

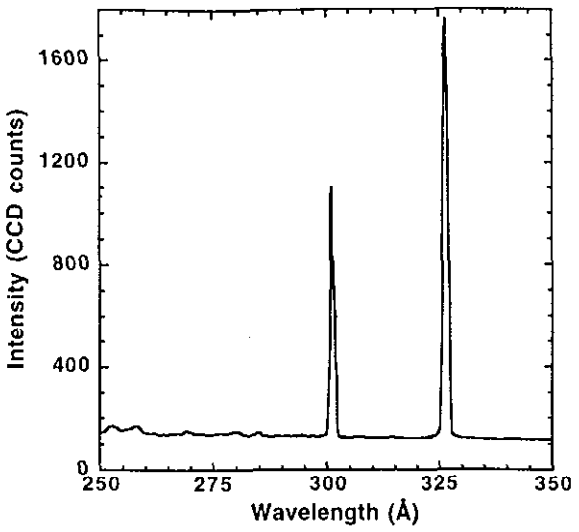

Fig2. Spectrum of Ne-like Ti showing lasing at 301 and 326 Å.

of the Ne-like ground state. The 285 Å line typically has half the gain of the 326 Å line because its oscillator strength is smaller by a factor of 2. The other set of lines are the 3d $^1P_1$ $\rightarrow$ 3p $^1P_1$ line at 301 Å and the 3d $^1P_1$ $\rightarrow$ 3p $^3P_1$ line at 314 Å. Again, both lines share the same upper laser state which is populated primarily by photopumping on the strong 2p $^1S_0$ $\rightarrow$ 3d $^1P_1$ transition. Both lines are predicted to lase, with the gain on the 314 Å line about 25% lower because of its weaker oscillator strength. In experiments done at MBI and LLNL only the stronger monopole collisional and photopumped lines at 326 and 301 Å lines are observed and we will only discuss those two lines further in this paper.

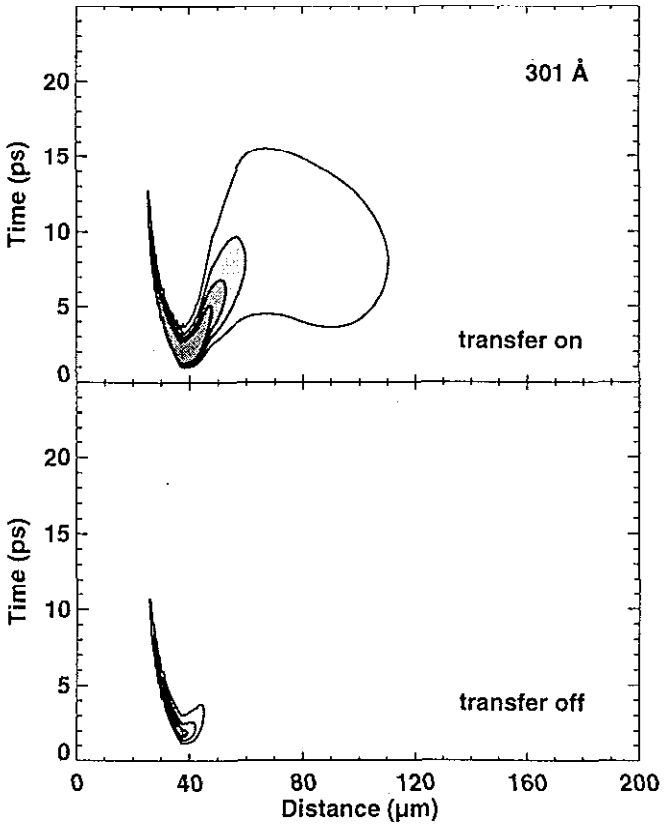

Fig. 3. Spatial and temporal evolution of the gain for the Ne-like Ti 301 Å laser line with line transfer turned on and off. Contours represent gain > 80, 60, 40, and 20 cm^{-1}.

Figure 1 shows contours of the gain versus space and time for the 326 Å and 301 Å laser lines for the nominal drive conditions described above. The short pulse laser peaks at 1 psec on this time scale so the evolution during the long pulse is not shown. The horizontal axis gives the distance from the target surface in the direction of the plasma expansion. The gain contours represent gains greater than 80, 60, 40, and 20 cm^{-1}. While the highest gain for the 326 Å line exceeds 200 cm^{-1} at 40 μm, which is near the critical density surface, just after the time of peak illumination, 2 psec, this gain region is very small and short lived and has steep gradients which would make it difficult to propagate any significant distance. If one looks at the 2nd gain contour with $g > 60$ cm^{-1} one can see that this region of large gain peaks about 80 μm from the target surface at about 8 psec, which is long after the short pulse laser has turned off. The gain lasts about 10 psec and extends over 50 μm. For the 301 Å laser line the gain region is somewhat shorter lived and has a smaller spatial extent. For both lines there is also a very narrow gain region which follows the critical density surface but that region is unlikely to allow laser propagation over any significant distance. Figure 2 shows a laser spectrum taken during an experiment at the COMET laser. One observes strong lasing on both the 326 and 301 Å laser lines. While the 326 Å line is very robust to changes in laser conditions the intensity of the 301 Å line is quite sensitive to small changes and its intensity varies a lot from shot to shot.

For the 301 Å laser line, one would normally not expect gain on this line because its upper laser state is the 3d $^1P_1$ level which is depopulated by the rapid radiative decay to the ground state via the strongest resonance line. However, in this plasma, the 2p $^1S_0 \rightarrow$ 3d $^1P_1$ line is optically thick and radiation trapping allows a very large radiation field to build up on this line and therefore populate the 3d $^1P_1$ upper laser state by radiative excitation (photopumping process). To understand the role of the self photopumping process on the gain of the Ne-like Ti laser lines, we did the XRASER calculations with the line transfer package turned off so that all the $n = 2 \rightarrow n = 3$ resonance lines are optically thin and the self photopumping process is absent. For the 326 Å laser line, looking 80 μm from the surface at 9 ps, there is a modest reduction of one-third in the gain. For the 301 Å laser line, Fig. 3 shows contours of the gain with line transfer on and off. In contrast to the 326 Å laser line, the gain of the 301 Å laser line disappears without the photopumping process except for a very small region near the critical density surface.

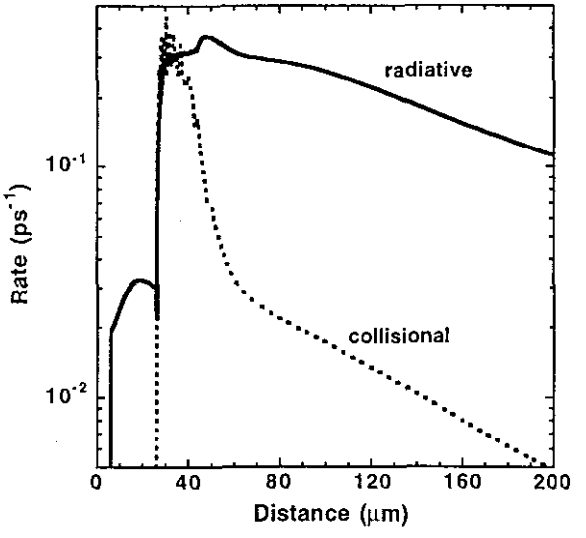

Fig. 4. Radiative and collisional rates on the ground state to 3d $^1P_1$ transition versus distance from target surface at 8.9 psec shows radiative processes driving the gain at 301 Å.

To better understand the role of the photopumping, Fig. 4 shows the collisional and radiative rates from the Ne-like ground state to the 3d $^1P_1$ upper laser state versus distance from the target surface at 8.9 psec. At 80 μm from the surface the radiative rate is more than an order of magnitude larger than the collisonal excitation rate. The collisional rate falls very rapidly with the electron density while the radiative rate depends on the photon density. While collisional excitations create the photons, the large optical depth of the 2p $^1S_0 \rightarrow$ 3d $^1P_1$ line, $\tau = 300$, allows photons which are created in the hot dense plasma near the surface and throughout the plasma to be trapped and contribute to the photopumping process.

One of the important parameters which affects the X-ray laser performance is the delay between the long and short pulse. Figure 5 shows the gain contours versus space and time for three different values of the delay, 0.6, 1.6, and 2.6 nsec. For the shortest delay of 0.6 nsec the gain has a small temporal and spatial extent near the critical density surface just after the time of peak laser illumination. Given the large gradients in the plasma one would not expect to see any significant lasing in this case. For the longest delay of 2.6 nsec, the gain duration is much longer but has a narrow spatial extent. In contrast, for the 1.6-nsec delay, the gain has both a large spatial and temporal extent. The electron density gradients are also smallest for the 1.6-nsec case, which allows the X-rays to propagate through the gain region and be amplified better. Figure 6 shows the electron density versus distance from target surface for the three cases at time zero, which is just before the short pulse laser turns on. During the short pulse laser illumination the hydrodynamics does not change much and the main change in electron density is just due to ionization.

Comparing the three different delays we do notice that the electron temperature becomes quite high for all three cases with peak values over 800 eV so this is not a limiting factor.

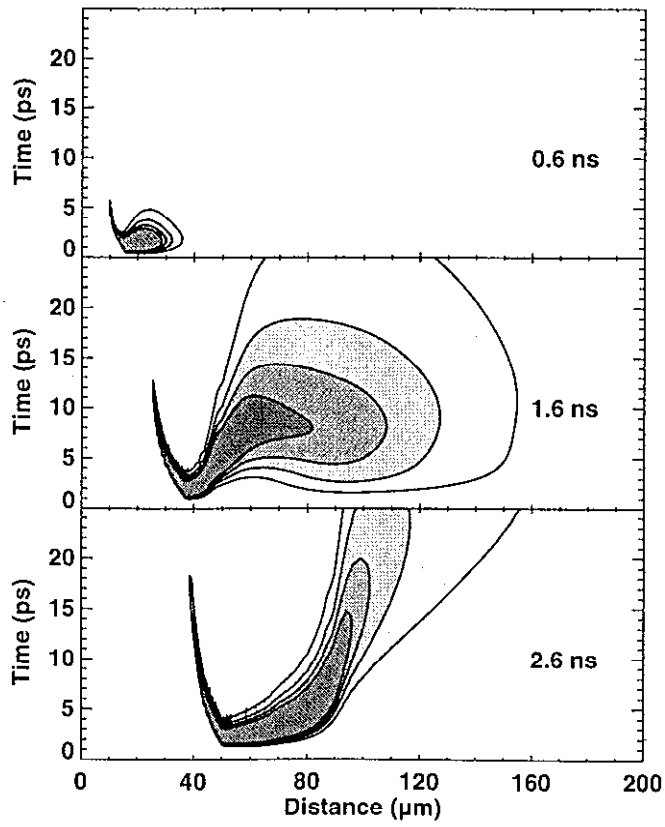

Fig. 5. Spatial and temporal evolution of the gain for the Ne-like Ti 326 Å laser line for three values of the delay between the long and short pulse drive lasers. Contours represent g > 80, 60, 40, 20 cm^{-1}. The short pulse laser peaks at 1 ps on this time scale.

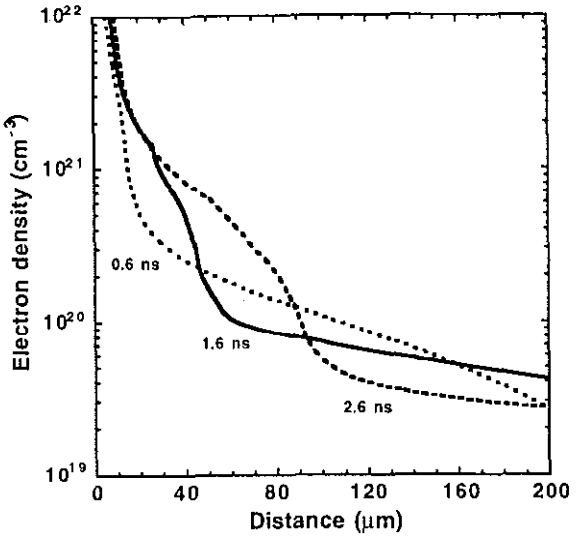

Fig. 6. Electron density versus distance at time zero just before the short pulse laser turns on for the three different delays between the long and short pulse laser.

The big difference between the cases is the ionization balance. Figure 7 shows the fraction of Ne-like Ti versus space and time for the three delays. Recall that the short pulse laser peaks at 1 psec on this time scale. The darkest contours represent Ne-like fraction greater than 50% with the other contours being 40, 30, and 20% fraction. For the 0.6-nsec delay the plasma tends to be overionized except at high densities. The long pulse over ionizes the plasma and the delay is too short to allow recombination to Ne-like. For the 2.6-nsec delay the plasma is underionized so that at time zero, before the short pulse laser is

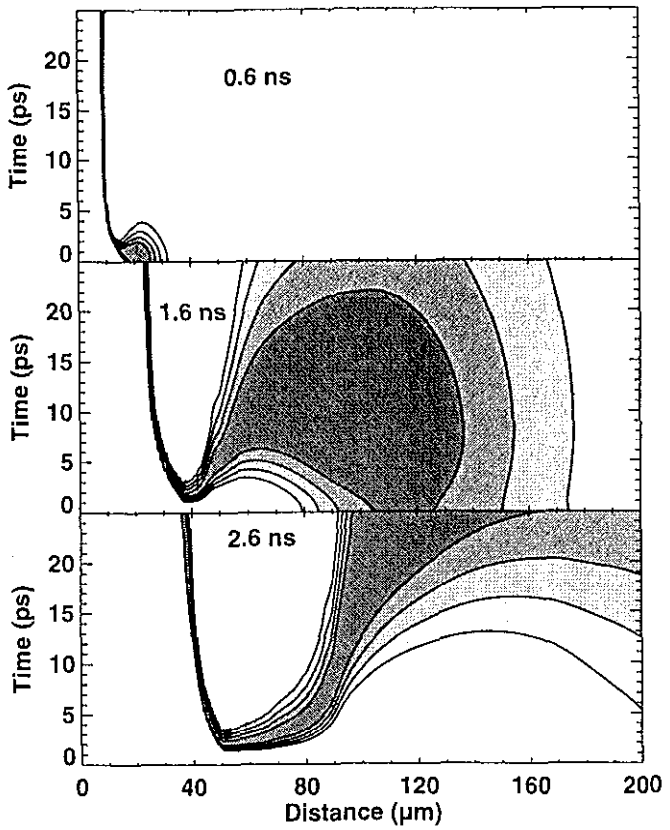

Fig. 7. Spatial and temporal evolution of the Ne-like ion fraction for the three different delays. Contours represent Ne-like fractions greater than 50, 40, 30, and 20%.

turned on, there is no Ne-like population except in the low-density region far from the gain region. In contrast, for the 1.6 nsec delay there is a large Ne-like population before the short pulse laser heats the plasma. It appears that the best delay is one that prepares the plasma with a large Ne-like population. The short pulse laser then can quickly heat the electrons, which drives the collisional excitation rate, without allowing time for the plasma to overionize.

For the optimum 1.6-nsec delay we also did calculations with different short pulse energy. If we double the short pulse energy to 12 J the gain increases and the region of high gain expands in time and space. Halving the energy to 3 J reduces the gain and shrinks the gain region. This is consistent with the idea that hitting a target harder makes it lase better. Given the long time duration for the gain compared with the 1 ps drive laser we also did a calculation where we kept the energy of the short pulse laser at 6 J but increased the pulse duration a factor of 5 to 5 ps. In that case we observed similar gain to the 1 ps drive case but the time duration of the gain increases slightly and the spatial extent decreases slightly. This suggests that a longer drive pulse should work just fine and that energy on target is the more important issue since we are operating in a regime where the gain duration is longer than the pulse duration of the drive laser. The longer pulse would have the advantage of relaxing the requirements on implementing the traveling wave geometry in the experiments. For example the use of stepped mirrors or tilted compressor gratings to make the traveling wave geometry introduce non-ideal features that might be less of a problem with the use of the longer pulse drive.

To understand the effect of refraction on the X-ray laser output we return to the case of the optimum 1.6 nsec delay. To study the refraction issue we consider a 1 cm long plasma which we illuminate from the end by a uniform source and then do a ray tracing calculation with amplification to determine the near field and far field laser intensity versus space and time. For simplicity we assume traveling wave illumination by the short pulse laser. Figure 8(a) shows the normalized intensity versus time. This has been integrated over space and angle. The laser output peaks at 8 psec with a FWHM duration of 1 psec. This shows that the gain region, which is contributing most to the output, is near 8 psec. If we now integrate over time Fig. 8(b) plots the laser intensity versus source position. This figure shows that X-rays, which start about 90 μm from the target surface, contribute most to the laser output. These X-rays start at 90 μm from the surface but are pointed inwards about 10 mrad so that

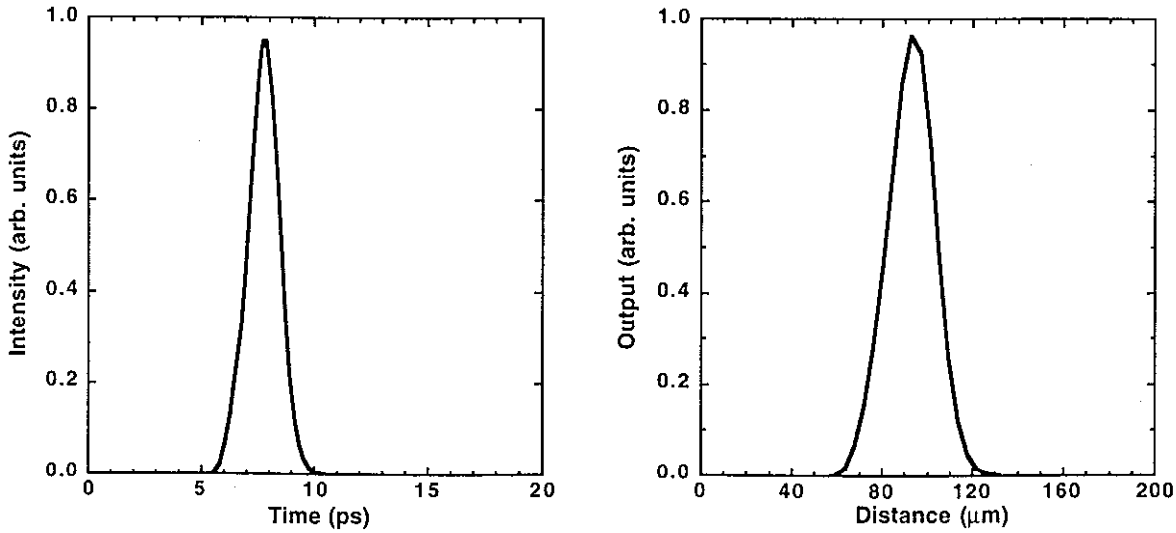

Fig. 8 Intensity versus time and output versus source position for a propagation calculation for the Ne-like Ti 326 Å laser line with 1.6 ns delay and 1 cm target length.

they sample gain even closer to the surface before they are refracted back out. More detailed propagation calculations are underway to better understand the refraction issues. If we look at the plasma 90 μm from the surface at 8 psec the electron density is 8.2×10^{19} cm^{-3} with an electron density gradient of -6.5×10^{21} cm^{-4}. A 326 Å photon propagating through down a 1 cm length with this gradient would be bent by 15 μm. The refraction effect is quite small in this region, which no doubt accounts for why it contributes so much to the laser output.

3. Conclusions

In this work we model recent experiments done using the COMET laser at LLNL to illuminate 1 cm long slab targets of Ti with a 4.8 J, 800 ps prepulse followed 1.6 nsec later by a 6 J, 1 psec drive pulse. The LASNEX code is used to calculate the hydrodynamic evolution of the plasma and provide the temperatures and densities to the XRASER code, which then does the kinetics calculations to determine the gain. The temporal and spatial evolution of the plasma is studied both with and without radiation transport included for the 3d and 3s → 2p Ne-like Ti resonance lines. Large regions with gain greater than 80 cm^{-1} are predicted for the 3p $^1S_0 \rightarrow$ 3s $^1P_1$ Ne-like Ti laser line at 326 Å. Given the large gain and large gradients in these plasmas, we do propagation calculations including refraction to understand which regions have the right combination of high gain and low gradients to contribute to the X-ray laser output. Calculations are also presented using different delays between the long and short pulse and different widths for the short pulse to provide better insight for optimizing the laser output. In addition to the standard 326 Å laser line, high gain is also predicted and observed for the 3d $^1P_1 \rightarrow$ 3p $^1P_1$ laser line at 301 Å in Ne-like Ti. We present calculations with and without radiation transport included on the strong 3d $^1P_1 \rightarrow$ 2p $^1S_0$ resonance line to better understand this self-photopumping effect.

We also expect the analog $3d^9$ 4f $^1P_1 \rightarrow 3d^9$ 4d $^1P_1$ transition in Ni-like ions to lase due to the self-photopumping mechanism and that has recently been observed at 226 Å in Ni-like Mo.

Acknowledgements – The authors would like to thank Richard Ward, Mark Eckart, and Luiz Da Silva for their support. Yuelin Li acknowledges support from Hector Baldis of the Institute for Laser Science and Applications (ILSA). Work performed under the auspices of the U. S. Department of Energy by the Lawrence Livermore National Laboratory under contract No.W-7405-ENG-48.

References

[1] J. Nilsen, B. J. MacGowan, L. B. Da Silva, and J. C. Moreno, Phys. Rev. A **48**, 4682 (1993).
[2] J. C. Moreno, J. Nilsen, and L. B. Da Silva, Opt. Comm. **110**, 585 (1994).
[3] P. V. Nickles, V. N. Shlyaptsev, M. Kalachnikov, M. Schnuerer, I. Will, and W. Sandner, Phys. Rev. Lett. **78**, 2748 (1997).
[4] J. Dunn, A. L. Osterheld, R. Shepherd, W. E. White, V. N. Shlyaptsev, and R. E. Stewart, Phys. Rev. Lett. **80**, 2825 (1998).
[5] J. Nilsen, Phys. Rev. A **53**, 4539 (1996).
[6] J. Nilsen, Phys. Rev. A **55**, 3271 (1997).